COBRA MANEUVER CONSIDERATIONS

Lars E. Ericsson[#]
Lockheed Missiles & Space Company, Inc.
Sunnyvale, California, USA

ABSTRACT

The unsteady aerodynamics associated with a rapid pitch-up/pitch-down motion of an advanced aircraft, the so called "Cobra" maneuver, have been analyzed. It is found that the maneuver could probably not be performed in laminar flow because of the expected nose-slice tendency based upon experimental results. The likely reason for the absence of nose-slice tendencies in full-scale flight is the existing coupling between boundary layer transition and vehicle motion. These results support the conclusion reached in earlier high-alpha analyses, i.e., dynamic simulation in subscale tests is only possible if the full-scale Reynolds number is simulated.

LIST OF SYMBOLS

b	wing span
c	reference length, $c = D$ or $c = d$
D	diameter in 2D flow
d	maximum body diameter in 3D flow
l	sectional lift, coefficient $c_l = l/q_\infty c$
N	coning rate
n	yawing moment, coefficient $C_n = n/q_\infty S\, b$
p	rotation rate
q_∞	dynamic pressure, $= \rho_\infty U_\infty^2/2$
Re	Reynolds number, $Re = U_\infty c/\nu_\infty$
S	reference area, $\pi d^2/4$ or projected wing area
t	time
Δt	time lag
U_∞	freestream velocity
U_W	wall velocity
x	axial distance from apex
Y	side force, coefficient $C_Y = Y/q_\infty S$
α	angle of attack
$\bar{\alpha}$	pitch-rate-induced angle at the nose tip, $\bar{\alpha} = x_{CG}\, \dot{\alpha}/U_\infty$
ν	kinematic viscosity
ρ	air density
ϕ	body-fixed roll angle
ψ	coning angle

SUBSCRIPTS

CG	center of gravity (rotation center)
W	wall
∞	freestream conditions

DERIVATIVE SYMBOLS

$$\dot{z} = \partial z/\partial t, \quad \ddot{\psi} = \partial^2\psi/\partial t^2$$

I. INTRODUCTION

The "COBRA" maneuver, performed by Pougachev at the 1989 Paris air show with the Soviet Su-27 "Flanker" [1](Figure 1), and later performed also with a MiG-29 at the Canadian National Air Show in Ottawa [2](Figure 2), requires lateral high-alpha stability superior to what until then had been demonstrated by other aircraft [3]. The obvious conclusion that has been drawn is that somehow symmetric flow separation has to be assured through the alpha range $0 < \alpha < 120°$. Some attention has been given to the problem of preventing the vortices from highly swept wing leading edges to generate large lateral loads in roll and yaw through asymmetric vortex breakdown and/or vortex lift-off [4,5]. However, nothing has been said about the potentially more serious lateral stability problem presented by asymmetric flow separation from a slender forebody[6] (Figure 3).

The lateral stability provided by the twin fins is probably comparable for the aircraft geometries shown in Figs. 1-3. The side forces generated on a slender nose[7] have a much larger lever arm for generation of a yawing moment (Figure 3) than what the vortex induced asymmetric loads generated on the wing leading-edge-extension have for generation of rolling and/or yawing moments (Figures 1 and 2). It is noted in Reference 3 that "the SU-27 radome does have small chines located at the apex of the nose. These chines are small but

#Retired. Presently Engineering Consultant

probably have a very positive effect on high AOA stability". As the chines are usually located at the lateral meridian to be effective[8], one should be able to spot them in the photographs of SU-27 and MiG-29 in Figures 1 and 2. Especially in the case of MiG-29 (Figure 2), one should be able to spot the presence of a chine near apex. That chines may not always be successful is demonstrated by low speed test results for conic noses[9] (Figure 4). In this test a nose boom was found to reduce the maximum side force $|C_Y|_{max}$ more than the lateral strakes near apex. However, this favorable nose-boom effect appears not to be present at higher Reynolds numbers[8,10] (Figure 5). Thus, not too much of an effect should be expected from the presence of nose booms on Su-27 and MiG-29 (Figures 1 and 2).

II. DISCUSSION

It has been found that the vortex wake from a very slender nose boom embeds the apex of the forebody, acting similarly to nose bluntness, thus delaying the start of asymmetric nose loads to a higher angle of attack[8]. Consequently, the experimental results for a blunted cone-cylinder geometry in rapid pitch-up motion[11](Fig. 6) should be of some relevance. The pitch-rate-induced angle of attack at the nose tip is $-\bar{\alpha} = -0.175 \approx -10°$. And for the pitch-down case (Fig. 7), the angle of attack is increased by 10°. Accounting for this pitch-rate-induced angle of attack gives the effective angle of attack $\alpha_N = (\alpha - \bar{\alpha})$ at the apex. Figure 8 shows that it did not fully account for the measured effect of the pitch rate on the boundaries between symmetric, asymmetric, and unsteady vortex shedding. However, if one adds the time lag for convection of the pitch-rate-induced effect from the nose to the local station x (Reference 12), giving the effective angle of attack $\alpha(x, t) = \alpha - \bar{\alpha}(1 + x/x_{CG})$, the prediction in Figure 8 will agree with the experimental data trend. Similar pitch-rate-induced effects have been observed on an ogive-cylinder model[13].

The message one obtains from the experimental results in Figures 6 - 8 is that the large side forces with associated huge yawing moments shown in Figure 3 should be realized also in a rapid pitching maneuver. The 70 deg./sec maximum pitch rate estimated for Su-27 (Reference 3) would induce angles of attack considerably lower than those covered in Figure 8. In addition, the coupling between crossflow separation and vehicle motion through so called moving wall effects[14] has been shown[15] to generate the driving moment for the observed coning motion of cone-cylinder bodies at high angles of attack[16], and to cause lateral oscillations of sting-mounted models in high-alpha tests[17].

In view of all the above facts, why did not the Su-27 and MiG-29 aircraft encounter lateral stability problems at high angles of attack? The obvious answer is that the discussed facts are for laminar flow conditions, giving high-alpha characteristics which apparently are very different from those existing in full-scale flight. Considering that we are almost totally dependent on experimental results for prediction of high-alpha separated flow characteristics, and that these experimental results often are obtained for laminar flow conditions, we obviously need to find an answer to the question stated above.

In the following section the coupling between the vehicle motion and the boundary layer transition/separation process is analyzed, and a hypothesis is presented which describes the fluid mechanics that could make the high Reynolds number lateral stability characteristics be so very different from those observed in subscale tests at laminar flow conditions.

II.1 Reynolds Number Sensitivity of Moving Wall Effects

The Reynolds number is one of the parameters that determines whether or not the flow separation is laminar. If it is above a certain critical value, which itself depends on things like surface roughness, freestream turbulence, etc., boundary layer transition will occur somewhere on the vehicle, thereby changing greatly the flow separation characteristics from what they are in purely laminar flow.

At high angles of attack one's concern is the effect of transition on the symmetric and especially the asymmetric flow separation with associated body vortices[7]. The experimental results[8] in Figure 9 show how powerful the moving-wall effects on laminar flow separation are. The authors describe how only a slight push was needed to establish the coning motion in the direction opposite to that determined by the nose micro-asymmetries[7], locking-in the vortex asymmetry in the direction of the coning motion, driving it until the vortex-induced yawing moment is balanced by the drag-generated damping moment (See top inset in Figure 9).

The laminar Magnus lift characteristics in Figure 10 at $U_W/U_\infty < 0.3$ supply the strip loads

for the coning, conical nose. Integrating the strip load contribution to the yawing moment gives the driving moment. It is balanced by the damping moment. generated by the drag, with c_d = 1.2 for laminar flow conditions. The resulting prediction[15] of the coning rate for $\alpha = 45°$ agrees well with the experimental results[8](Figure 11). The zero offset is caused by bearing friction present in the test, which was not included in the prediction(as it was not known).

The moving wall effect on flow separation via transition is responsible for the oscillatory coning observed on the cone-cylinder body in Figure 9, when it was turned around 180 deg.[7] (Figure 12). The Magnus lift reversal observed on a circular cylinder[18] illustrates this (Figure 10). The positive Magnus lift, at $U_W/U_\infty < 0.3$, is caused by the wall-jet-like downstream moving wall effect on the top side, which fills out the boundary layer velocity profile, thereby delaying flow separation. A similar lift-contribution is obtained from the upstream moving wall effect on the bottom side, which promotes separation. At $U_W/U_\infty > 0.3$, so called Magnus lift reversal occurs. This is caused by the upstream moving wall effect on the bottom side, which, when the critical U_W/U_∞- Reynolds number combination is exceeded, will cause boundary layer transition to occur upstream of flow separation, thereby changing the separation from the subcritical towards the supercritical type. This results in a more or less discontinuous loss of lift. As the moving wall effect is of significant magnitude only in the region near the stagnation point[19], these results for the rotating cylinder apply also to the translating cylindrical cross-section in Figure 12.

Initially, flow asymmetry or surface irregularities set the vortex asymmetry. The resulting coning motion reinforces the effects of the asymmetry, as the laminar separation is delayed on the advancing side. Positive coning velocity and acceleration result ($\dot\psi$ and $\ddot\psi > 0$). However, as $\dot\psi$ increases, the moving wall effect eventually causes boundary layer transition forward of flow separation on the retreating side. This reverses the vortex asymmetry (as in the case of the Magnus lift reversal in Figure 10) and the coning motion starts to decelerate ($\dot\psi > 0$ but $\ddot\psi < 0$). Eventually, this results in accelerated coning in the opposite direction ($\dot\psi$ and $\ddot\psi < 0$). The rotation reversal moves transition back into the wake on the new advancing side, and asymmetric laminar separation is re-established.

Eventually, transition occurs on the retreating side to cause critical/subcritical flow separation, reversing the asymmetry and the coning motion is decelerated ($\dot\psi < 0$, $\ddot\psi > 0$). The process continually repeats itself, resulting in a self-reversing coning motion with limit rates in both directions similar to the $\dot\psi(\alpha)$ characteristics shown in Figure 9.

A similar moving wall effect generated by body spin is responsible for the wing rock observed on a generic aircraft configuration[20] (Figure 13). This wing rock is even more violent than the one observed on a 80° delta wing[21] (Figure 14). Also in this case asymmetric vortex shedding is observed[20]. However, instead of the direct effect of the lifted-off leading-edge vortex on the slender delta wing[22,23], the wing surfaces on the generic configuration are not directly involved in the asymmetry-switching process but are only present to respond to the flow field generated by the forebody vortices[24] (Figure 15). The crossflow over the nose-cylinder shoulder was in the critical Re-region, providing the following scenario: At $t=t_1$, the wing-body (removing the tail surfaces had little impact on the wing rock motion) is rolling in response to some disturbance. The generated adverse, upstream moving wall effect on the right, starboard side causes transition to occur in the forebody crossflow ahead of separation, changing it from the subcritical towards the supercritical type in the manner discussed earlier in connection with Figure 10. On the opposite side the favorable, downstream moving wall effect delays transition, reinforcing the subcritical nature of the flow separation on this side. This description is somewhat oversimplified, as it neglects the presence of the laminar separation bubble.

Neglecting time lag effects, the vortex geometry sketched at $t = t_1$ would result. Due to time lag effects, similar to those discussed in Reference 22, this vortex geometry* is not realized until $t = t_1 + \Delta t$. At $t \leq t_3$, when the roll rate approaches its maximum in the opposite direction, another forebody switch in separation asymmetry occurs. Because of the time lag effect, the vortex geometry at the (now horizontal) wing has not changed, but is the same as at $t = t_1 + \Delta t$, in agreement with the flow pictures in Reference 20. The much faster amplitude build-up (Figure 13) than for the slender delta wing

_____

*Only the lower vortex is shown as only it will induce significant loads on the wing-body.

(Figure 14) is caused by the half cycle to half cycle increase of the separation asymmetry due to the increasing moving wall effects[24]. At α >40°, free flight tests of a 1/3 scale model of the X-29A configuration shows this type of wing rock[25], in addition to the one generated by dynamic wing-stall at 20° < α < 30° (Reference 26 and Figure 16).

This wing rock generated by forebody vortices cannot materialize unless the critical flow condition can be established. Thus, in a test in a low Reynolds number facility, producing laminar flow conditions over the forebody, this type of wing rock will not be discovered. On the other hand, in a test in a facility capable of higher Reynolds numbers, but still substantially below full scale values, the conditions existing in the test described in Reference 20 can be established. That is, the critical flow conditions are created near the nose-cylinder juncture for an ogive-cylinder forebody (or at an equivalent region on an arbitrary, slender forebody). This generates the maximum possible wing rock amplitude, whereas at full-scale flight conditions the critical flow condition is established much farther forward, near the apex of a slender forebody, where the separation-induced vortices will be of lesser strength[24,27].

In searching for a physical explanation of the troublefree "Cobra" maneuver in full-scale flight one can propose the following based upon the experimental results presented so far: Increasing the Reynolds number will always reduce the potential for side force generation as the projected area over which a separation asymmetry can be established is smaller at supercritical than at subcritical crossflow conditions (See flow sketches in Figure 10). However, a side force with associated nose-slice tendency will still materialize. The most important difference in the fluid mechanics caused by increasing the Reynolds number above the critical value is the establishing of the coupling between transition and vehicle motion. As is illustrated by the results in Figures 9-12, this can reverse the effect of flow separation from what it is in laminar flow. Thus, instead of driving the coning (nose-slicing) motion, as in the case of laminar flow (Figure 11), the flow separation in the critical (Reynolds number) region will have the reverse effect, i.e., it will damp any coning or nose-slicing motion. Note that as the Reynolds number is increased, the U_W/U_∞ value for the reversal decreases (Figure 10). One would expect this damping effect of the separation reversal to vary with Reynolds number, similarly to how the corresponding

undamping effect on wing rock varies[24,27]. The absence of nose-slicing tendencies in the X-29A wing rock motion[25] is in perfect agreement with the fluid mechanic processes postulated here, which affect coning and wing rock motions in opposite ways. As the Reynolds number is increased and the critical crossflow region moves closer to the nose tip, the yaw-damping effect of the reversal will diminish. However, it will still be present, as was demonstrated in the case of wing rock[26], supplying a logic explanation for the absence of nose-slice tendencies in the performed "Cobra" maneuvers. The results discussed above supply a sobering reminder of the fact that dynamic simulation of high-alpha vehicle dynamics is not possible unless the full-scale Reynolds number is simulated[28,29].

III. CONCLUSIONS

Analysis of available experimental results leads to the following conclusions:

1. The "Cobra" maneuver could not be performed in laminar flow.

2. The coupling between boundary layer transition and vehicle motion appears to be the most likely reason for the absence of nose-slice tendencies when performing the "Cobra" maneuver at full-scale Reynolds numbers.

3. The above statements reinforce the conclusion drawn from similar analyses in the past, i.e., dynamic simulation in subscale tests is not possible unless the full-scale Reynolds number is simulated.

IV. ACKNOWLEDGEMENT

V. REFERENCES

1. Aviation Week, Sept. 24, 1990.

2. Aviation Week, July 9, 1990.

3. Skow, A. M., "An Analysis of the Su-27 Flight Demonstration at the 1989 Paris Airshow", SAE Technical Paper No. 901001, April 1990.

4. Cunningham, A. M. Jr. and Bushlow, T., "Steady and Unsteady Force Testing of Fighter Aircraft Models in a Water-Tunnel", AIAA Paper 90-2815-CP, Aug. 1990.

5. Manor, D., Miller, L., Wentz, W. H. Jr, "Static and Dynamic Water Tunnel Tests of Slender Wings and Wing-Body Configurations at Extreme Angles of Attack", AIAA Paper 90-3021, Aug. 1990.

6. McElroy, G. E. and Sharp, P. S., "An Approach to Stall/Spin Development and Test", AIAA Paper NO. 71-772, July 1971.

7. Ericsson, L. E., and Reding, J. P., "Asymmetric Vortex Shedding from Bodies of Revolution", Chapter VII, Tactical Missile Aerodynamics, Vol. 104 of Progress in Astronautics and Aeronautics Series, edited by J. M. Hemsch and J. N. Nielsen, Sept. 1986, pp. 243-296.

8. Ericsson, L. E. and Reding, J. P., "Alleviation of Vortex-Induced Asymmetric Loads", J. Spacecraft and Rockets, Vol. 17, Nov.-Dec. 1980, pp. 546-553.

9. Modi, V. J., Ries, T., Kwan, A., and Leung, E., "Aerodynamics of Pointed Forebodies at High Angles of Attack", J. Aircraft, Vol. 21, June 1984, pp. 428-432.

10. Keener, E. R. and Chapman, G. T., "Onset of Aerodynamic Side Forces at Zero Sideslip on Symmetric Forebodies at High Angles of Attack", AIAA Paper 74-770, Aug. 1974.

11. Montevidas, R. E., Reisenthel, P. and Nagib, H. M., "The Scaling and Control of Vortex Geometry Behind Pitching Cylinders", AIAA Paper 89-1003, March 1989.

12. Ericsson, L. E., "Unsteady Flow Separation on Slender Bodies at High Angles of Attack", AIAA Paper 90-2835, August 1990.

13. Gad-el-Hak J. M. and Ho, C-M., "Unsteady Flow Around an Ogive Cylinder", J. Aircraft, Vol 23, June 1986, pp. 520-528.

14. Ericsson, L. E., "Moving Wall Effects in Unsteady Flow", J. Aircraft, Vol. 25, Nov. 1988, pp. 977-990.

15. Ericsson, L. E., "Prediction of Slender Body Coning Characteristics", J. Spacecraft and Rockets, Vol. 28, Jan.-Feb. 1991, pp. 43-49.

16. Yoshinaga, T., Tate, A., and Inoue, K., "Coning Motion of Slender Bodies at High Angles of Attack in Low Speed Flow", AIAA Paper 81-1899, Aug. 1981.

17. Ericsson, L. E., "Lateral Oscillations of Sting-Mounted Models at High Alpha", J. Spacecraft and Rockets, Vol. 27, Sept.-Oct. 1990, pp. 508-513.

18. Swanson, W.M., "The Magnus Effect: A Summary of Investigations to Date", J. Basic Engineering, Vol. 83, pp. 461-470.

19. Ericsson, L.E.,"Circular Cylinder Response to Karman Vortex Shedding", J. Aircraft, Vol.25, Sept. 1988, pp. 769-775.

20. Brandon, J. M. and Nguyen, L. T., "Experimental Study of Effects of Forebody Geometry on High Angle of Attack Static and Dynamic Stability", J. Aircraft, Vol. 25, July 1988, pp. 591-597.

21 Nguyen, L., Yip, L. and Chambers, J.,"Self-induced Wing Rock of Slender Delta Wings", AIAA Paper 81-1883, Aug. 19-21, 1981.

22. Ericsson, L. E., "The Fluid Mechanics of Slender Wing Rock", J. Aircraft, Vol. 21, May 1984, pp. 322-328.

23. Ericsson, L. E., "Analytic Prediction of the Maximum Amplitude of Slender Wing Rock", J. Aircraft, Vol. 26, Jan. 1989, pp. 35-39.

24. Ericsson, L. E., (1987) "Wing Rock Generated by Forebody Vortices", J. Aircraft, Vol. 26, Feb. 1989, pp. 110-116.

25. Fratello, D. J., Croom, M. A., and Nguyen, L. T., "Use of the Updated NASA Langley Radio-Controlled Drop-Model Technique for High-Alpha Studies of the X-29A Configuration", AIAA Paper 87-2559-CP, Aug. 11987.

26. Ericsson, L.E.,"Prediction of High-Alpha Vehicle Dynamics", ICAS-90-3.5.1, Sept. 1990.

27. Ericsson, L. E., "Further Analysis of Wing Rock Generated by Forebody Vortices", J. Aircraft, Vol. 26, Dec. 1989, pp. 1648-1650.

28. Ericsson, L.E. and Reding, J.P., "Scaling Problems in Dynamic Tests of Aircraft-Like Configurations", Paper 25, AGARD-CP-227, 1978.

29. Ericsson, L.E., "Effects of Transition on Wind Tunnel Simulation of Vehicle Dynamics", Progress in Aerospace Sciences, Vol. 27, pp. 121-144, 1990.
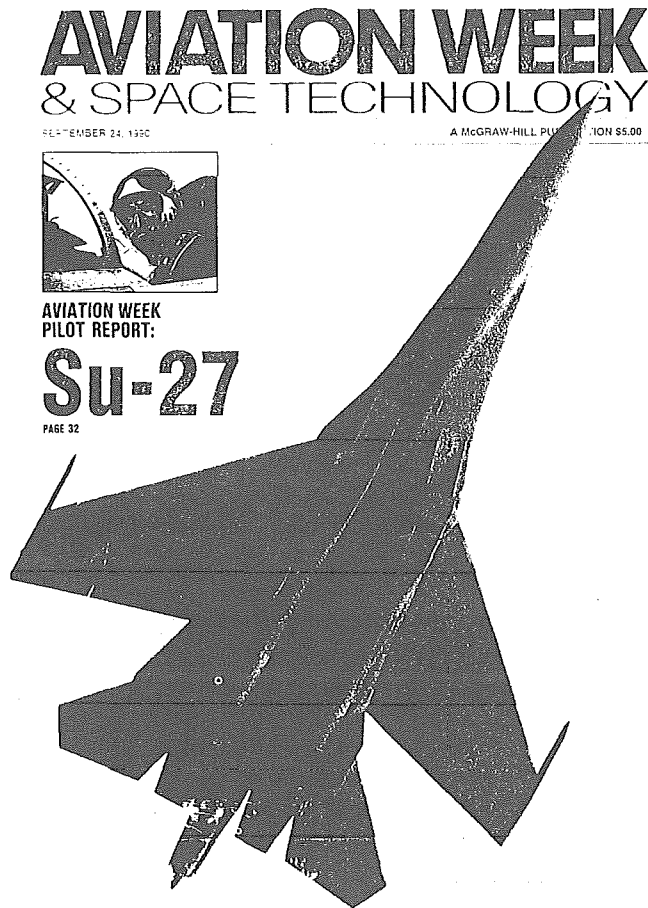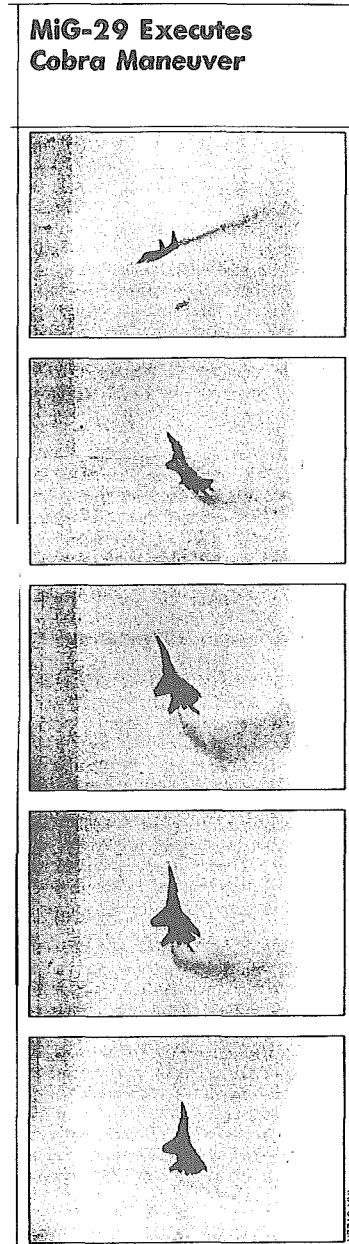
MiG-29 Executes Cobra Maneuver

Fig. 1   SU-27 Configuration (Ref. 1).

Fig. 2   MiG-29 Configuration (Ref. 2).

THREE-VIEW SKETCH OF CONFIGURATION WITH LONG
POINTED NOSE

a. VARIATION OF YAWING-MOMENT COEFFICIENT WITH
ANGLE-OF-ATTACK, SYMBOLS INDICATE VALUES OBTAINED
IN SEVERAL REPEAT TESTS

b. VARIATION OF STATIC YAWING-MOMENT COEFFICIENT
WITH ANGLE-OF-ATTACK FOR SEVERAL MODELS OF THE
CONFIGURATION
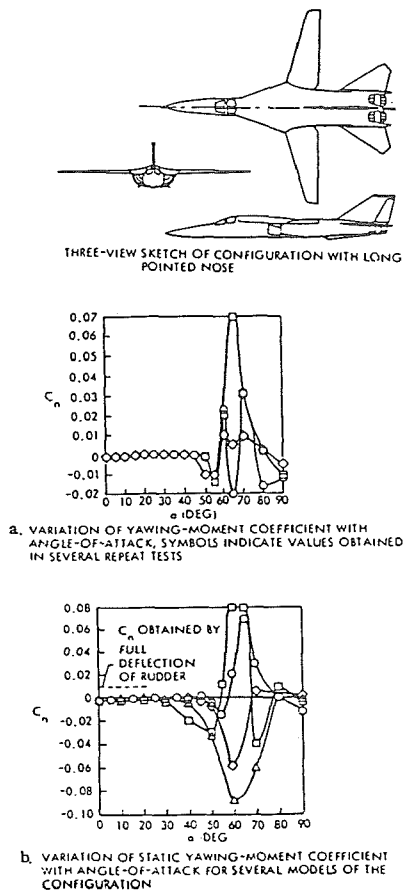
Fig. 3   Yawing Moment Measured at Zero
Sideslip on Slender Nose Aircraft at
High Angles of Attack (Ref. 6).
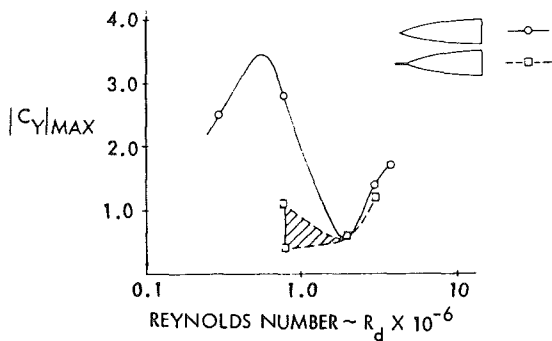
Fig. 5   Effect of Nose Boom on Measured
Maximum Side Force (Ref. 8).
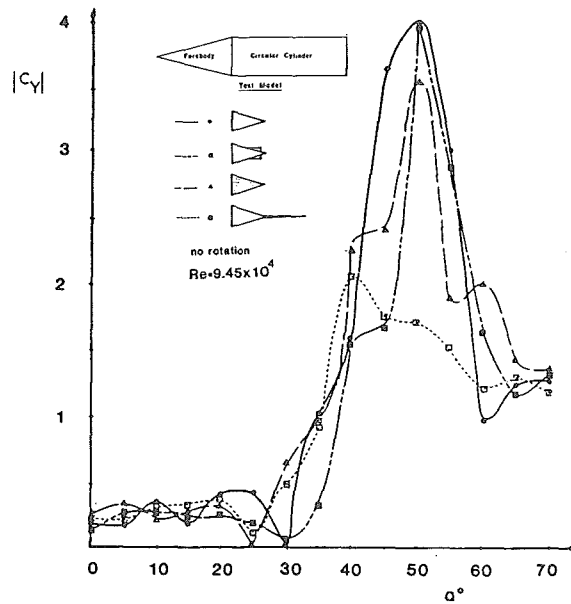
Fig. 4   Effect of Nose Tip Geometry on
Measured Side Force (Ref. 9).
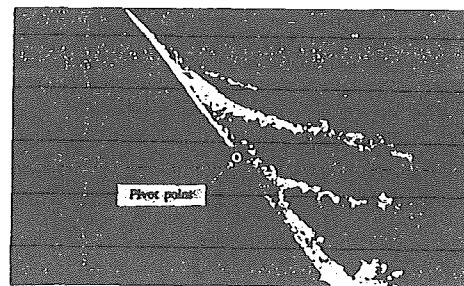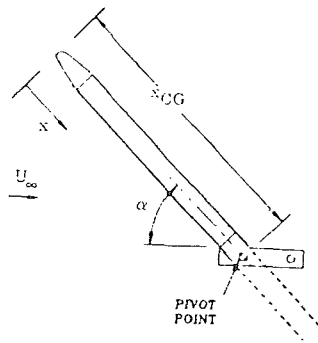
$\alpha = 55°$

$\bar{\alpha} = .175$

Fig. 6   Asymmetric Vortices on Cone-Cylinder
Body in Pitch-Up Motion (Ref. 11).
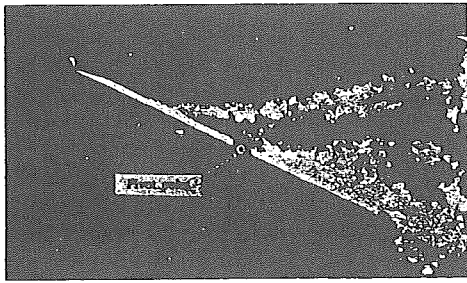
$$\alpha = 25°$$
$$\bar{\alpha} = -.175$$

Fig. 7 Asymmetric Vortices on Cone-Cylinder Body in Pitch-Down Motion (Ref. 11).

Pitch down ← | Pitch up →

L/D = 10.3

Unsteady

Asymmetric

Symmetric Attached

Lines of constant effective angle

Fig. 8 Effective Angle of Attack as a Function of Reduced Pitch Rate (Ref. 12).

C.G.=50 %

$a = 45°$ 50° 55° 60°

o U_∞ INCREASED
x U_∞ DECREASED
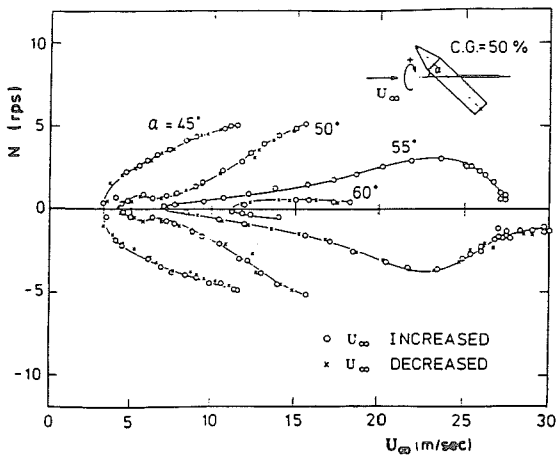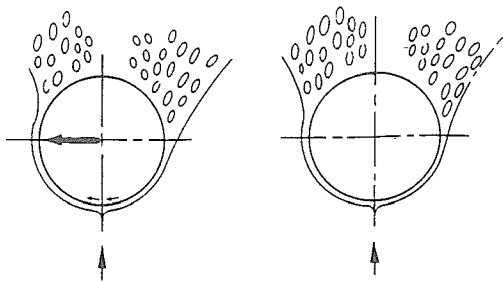
Fig. 9 Dual Coning Characteristics of a Cone-Cylinder Body (Ref. 16).

p = 0

p >> CRIT.

TRANSITION

CURVE	Re ×10⁻⁴

p < CRIT.

p ≅ CRIT.

TRANSITION
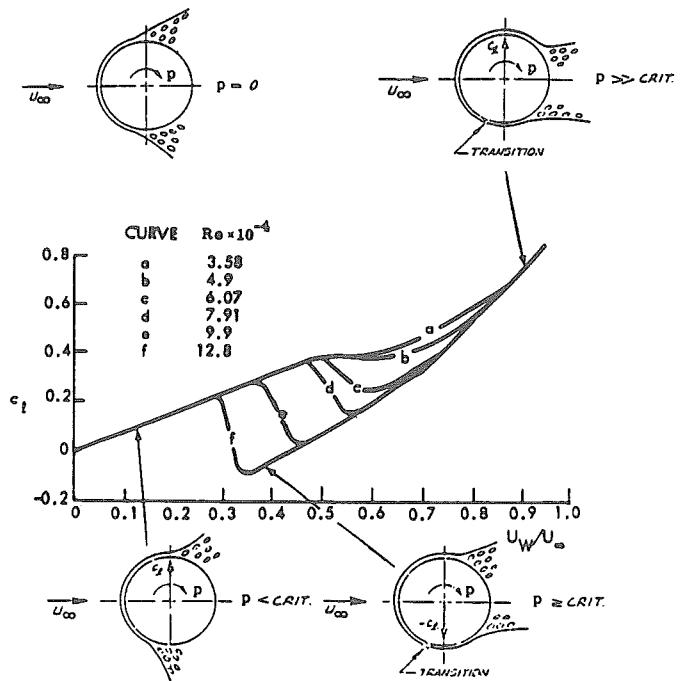
Fig. 10 Magnus Lift Characteristics for Initially Laminar Flow Conditions (Ref.18).
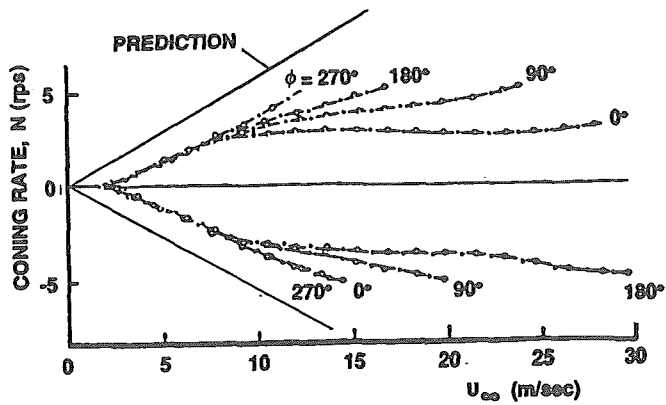
Fig. 11 Coning Characteristics of a Cone-
         Cylinder Body.
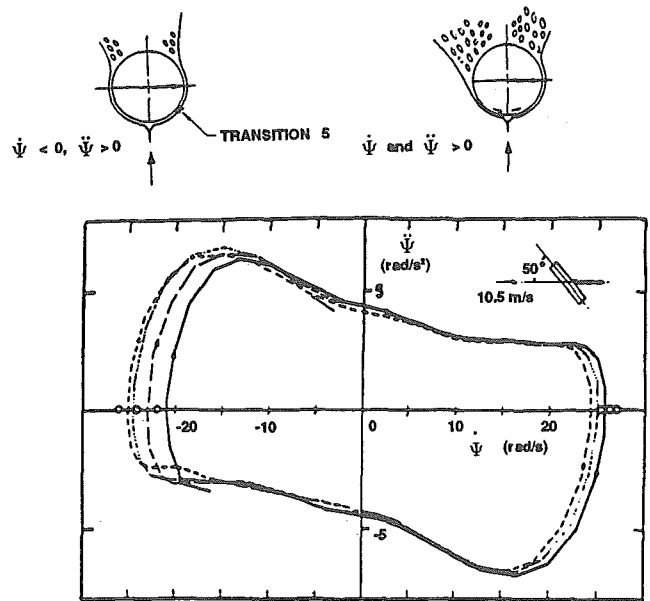
Fig.12 Acceleration/Rate Time History of a
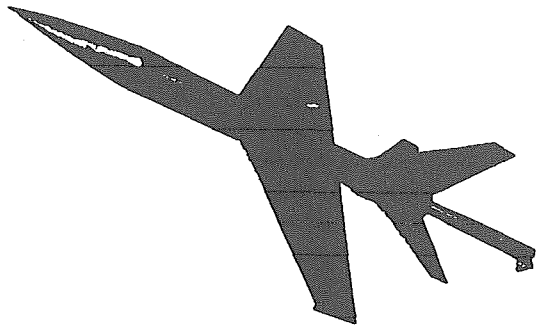   Flat-Faced Circular Cylinder Coning at
        $\alpha = 50°$.
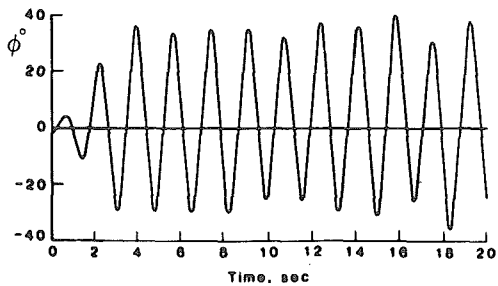
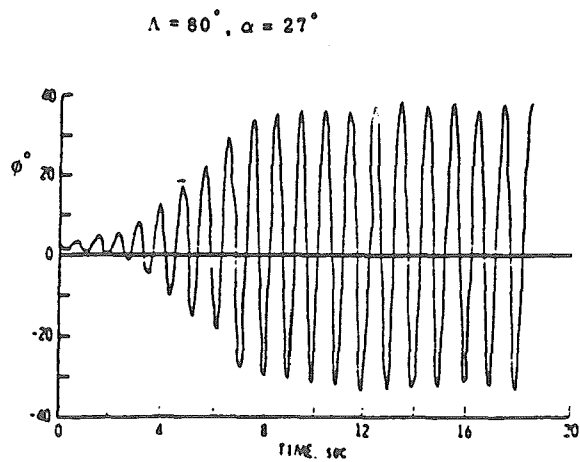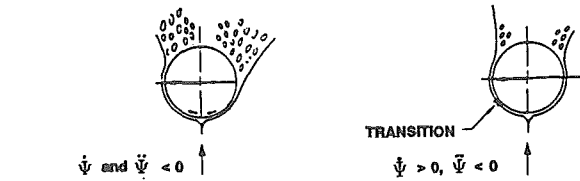Fig. 13 Wing Rock Build-Up at $\alpha = 30°$ (Ref. 20).

Fig.14 Wing Rock of Sharp-Edged 80° Delta
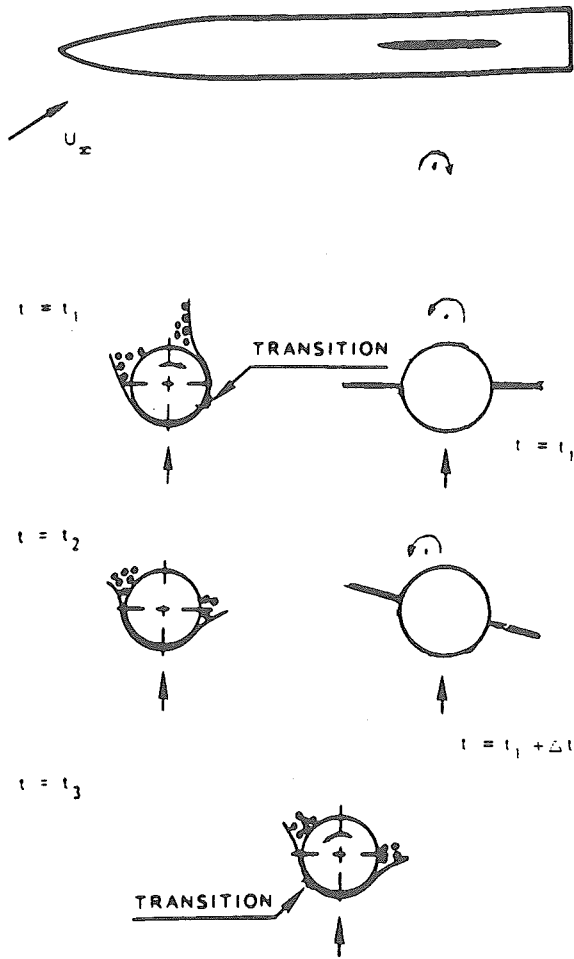   Wing (Ref. 21).

1223

Fig. 15 Conceptual Flow Mechanism for
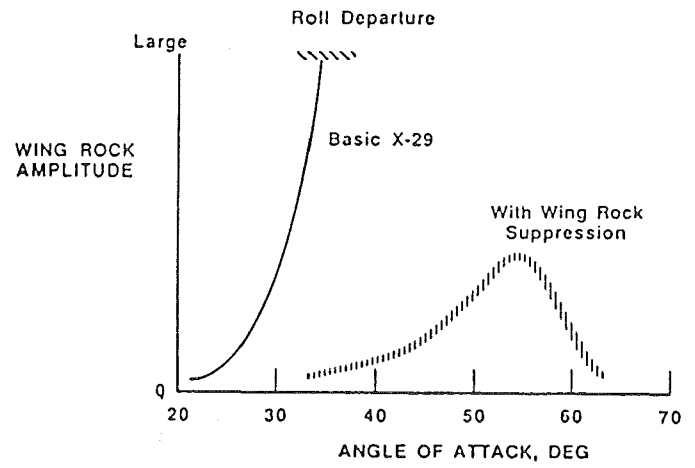Forebody-Induced Wing Rock (Ref. 24).

Fig. 16 Wing Rock Characteristics of the X-29
Aircraft (Ref. 25).